

ELVIS: Enhance Low-light for Video Instance Segmentation in the Dark

Joanne Lin Ruirui Lin Yini Li David Bull Nantheera Anantrasirichai
University of Bristol

{joanne.lin, r.lin, ub24017, dave.bull, n.anantrasirichai}@bristol.ac.uk

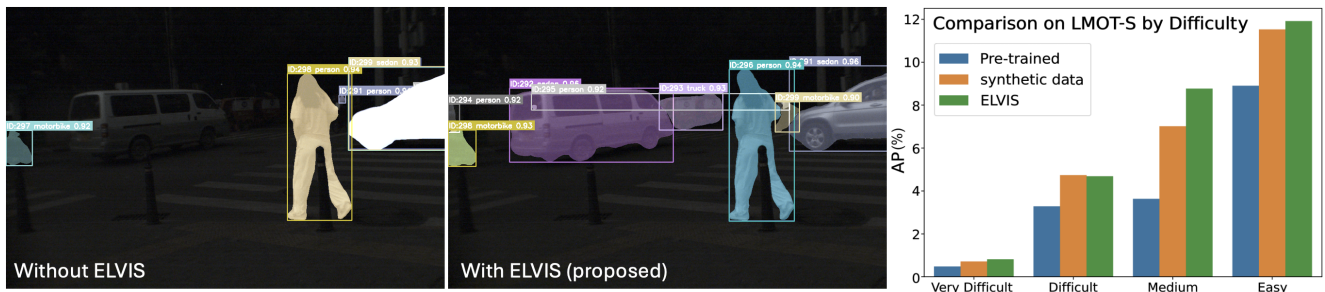


Figure 1. **Video Instance Segmentation (VIS) in real low-light conditions.** Comparison of results using (left) GenVIS [15] and (middle) GenVIS+ELVIS. (Right) Quantitative performance comparison between the pre-trained VIS method, re-trained with synthetic low-light data, and the proposed ELVIS framework across different levels of difficulty.

Abstract

Video instance segmentation (VIS) for low-light content remains highly challenging for both humans and machines alike, due to adverse imaging conditions including noise, blur and low-contrast. The lack of large-scale annotated datasets and the limitations of current synthetic pipelines, particularly in modeling temporal degradations, further hinder progress. Moreover, existing VIS methods are not robust to the degradations found in low-light videos and, as a result, perform poorly even when finetuned on low-light data. In this paper, we introduce **ELVIS** (Enhance Low-light for Video Instance Segmentation), a novel framework that enables effective domain adaptation of state-of-the-art VIS models to low-light scenarios. ELVIS comprises an unsupervised synthetic low-light video pipeline that models both spatial and temporal degradations, a calibration-free degradation profile synthesis network (VDP-Net) and an enhancement decoder head that disentangles degradations from content features. ELVIS improves performances by up to **+3.7AP** on the synthetic low-light YouTube-VIS 2019 dataset. Code will be released upon acceptance.

1. Introduction

Video instance segmentation (VIS) is a challenging yet important task in computer vision; with the goal of not only

detecting, classifying and tracking an object, but also determining the pixel mask of the object. This enables a fine-grained understanding of the object’s state and motion. The task becomes even more complex under low-light conditions, which are common in applications including autonomous driving, wildlife conservation, surveillance, post-production and robotics.

Few datasets exist specifically for low light data, reflecting the limited amount of research in this field. One contributing factor is that degradations caused by low-light conditions pose challenges for both human and automated annotation, as creating high-quality annotations for downstream tasks requires considerable effort. In particular, only a limited number of publicly available benchmarks [21, 23, 27, 39, 43] exist for downstream tasks in low-light videos, and none of them are specifically designed for VIS applications.

Due to the scarcity of adequate training data, two main strategies are commonly employed to improve the performance of downstream tasks on low-light images and videos. One approach is to apply a pre-trained low-light enhancement method [3, 5, 26, 38] to the data as a pre-processing step; however, low-light *video* enhancement itself is still in its infancy. The other approach is to synthesize appropriate low-light conditions by modifying existing datasets for training [9, 23, 24, 44]; these are commonly used to enable an end-to-end approach for downstream tasks in the

dark. Most existing synthetic approaches have been developed primarily for *images*, reflecting the greater development and maturity of low-light image research. However, these methods often do not account for the blur degradations present in low-light videos, which result from the longer shutter speeds required to capture the content.

Furthermore, existing downstream methods are not designed to be robust to the degradations present in such conditions. Some works [9, 11, 24] focus on modifying architectures to improve robustness to degradations, others [2, 23, 42] leverage alternative data (such as RAW data and events) for richer scene context, and [7] combine both strategies. None of these, however, explore domain adaptation for VIS tasks in the dark.

To address these limitations, we propose a new synthetic low-light video pipeline and a framework (ELVIS) for improving the performance of existing VIS methods on low-light videos without the need for alternative data. An example of ELVIS’s capabilities is shown in Fig. 1. Our contributions are three-fold:

- We introduce the **first** low-light Video Instance Segmentation (VIS) method, **ELVIS**, which integrates a pixel-decoder enhancement module into existing VIS architectures to disentangle degradation features from scene content, thereby boosting their performance in low-light videos.
- We develop the **first** physics-based degradation model for synthesizing **low-light videos**, incorporating illumination adjustment, blur degradations, and camera noise.
- We propose a novel unsupervised Video Degradation Profiler Network (VDP-Net), trained in an unsupervised manner to accurately estimate degradation profiles, enabling calibration-free synthesis of real low-light videos.

2. Related Work

2.1. Synthetic Low-Light Pipelines

Physics-based pipelines. One popular synthetic low-light pipeline from Lv *et al.* [30] considers the noise as a result of demosaicing in addition to read and shot noise. They make use of the heteroscedastic noise model [12], which uses a Gaussian distribution as an approximation for combining read and shot noise (often modeled separately using a Gaussian and Poisson distribution). Although this is a sufficient approximation for brightly-lit conditions, it fails to accurately model read and shot noise in low-light conditions [37]. Many works exploring low-light downstream tasks [23, 24, 46] make use of this synthetic pipeline for their research, due to its simplicity and versatility.

Wei *et al.* [40] propose a RAW noise pipeline which involves meticulous experimentation with camera-metadata for collecting the noise parameters for their proposed noise model. They calculate the noise profiles for 5 different

cameras using statistical methods. Their synthetic pipeline models the following noise types using various statistical distributions: read noise, shot noise, quantization noise, and banding noise. This work has been used by Chen *et al.* [7] for instance segmentation in RAW low-light images.

Deep-learning pipelines. Building upon physics-based methods, Monakhova *et al.* [31] designed a Wasserstein GAN [1] to synthesize bursts of noisy RAW frames from a clean still RAW image. The generator learns to first estimate the degradation parameters of their Submillilux dataset, followed by a U-Net [35] to further model complex degradations. While effective for their dataset, the method lacks generalizability and requires re-training for other use cases. Meanwhile, Zhou *et al.* [50] explored a multi-step approach to synthesizing low-light sRGB videos which considered illumination, blur and noise degradations. However, their method still has limitations as they incorporate supervised methods [33, 45] for synthesizing the degradations.

2.2. Calibration-free Degradation Estimation

Several works have explored estimating degradations within images and videos, particularly noise, for calibration-free, physics-based synthesis. Jin *et al.* [18], Zou *et al.* [52], and Lin *et al.* [25] adopt approaches similar to ours by leveraging physics-based statistical distributions to synthesize noise, though each have notable limitations. Jin and Zou *et al.* rely on the manually collected degradation parameters from [40] to train their noise estimation model. This requires image-capture metadata such as camera model and ISO, which are typically unavailable in publicly released datasets used for downstream tasks. Lin *et al.* address this issue by training a U-Net [35] to estimate degradation parameters across diverse noise distributions; however, their method is tailored towards extreme low-light noise.

2.3. Domain adaptation via synthetic data

Many works [23, 24, 42, 46] use pre-existing pipelines for synthesizing their training data for downstream tasks under low-light conditions, while others propose their own synthetic pipelines [9, 29]. These synthetic methods generally have lower complexity; prioritizing efficiency over photorealism, to achieve on-the-fly synthesis for greater variability during training. Cui *et al.* [9] explores synthesizing degradations resulting from in-camera processing. Using the unprocessing algorithm from [4], they convert the data from sRGB into RAW format, inject read and shot noise (modeled with Gaussian and Poisson distributions respectively), and reconstruct the sRGB images via a simple ISP pipeline. They incorporate this low-light pipeline within their training objective, by jointly learning to predict the degradation parameters to synthesize the input, and the object detection predictions. Du *et al.* [11] make use of the proposed pipeline from [9] in their works, but approach domain adap-

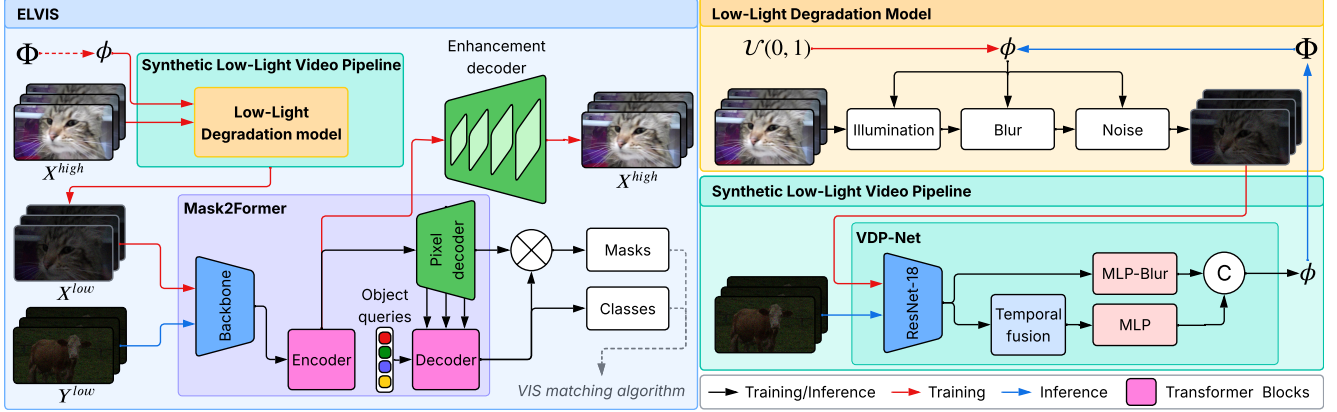


Figure 2. Overview of the proposed ELVIS framework, which consists of two main components: (i) the unsupervised synthetic low-light pipeline and (ii) the augmented instance segmentation module. The synthetic low-light video pipeline (green panel) degrades clean videos X^{high} using the low-light degradation model (yellow panel) and degradation parameters ϕ estimated by VDP-Net.

tation differently by passing the normal-light image and the synthesized low-light image into the network to learn to predict both detections and extracting the reflectance components from the inputs (from the Retinex theory [20]). Similarly, Chen *et al.* [7] uses for synthesizing low-light images. They first ‘unprocess’ the sRGB images into RAW format using the method proposed by [4] and then applies Wei *et al.*’s [40] noise model to synthesize low-light RAW images.

3. Methodology

An overview of the proposed Enhanced Low-light for Video Instance Segmentation (ELVIS) framework is shown in Fig. 2. The ELVIS framework introduces two novel components: (i) an unsupervised Synthetic Low-Light Pipeline, detailed in Sec. 3.1, and (ii) an Enhancement Decoder Head within the VIS network, which reconstructs the original video and thereby improves the perceptual capability of VIS methods under low-light conditions, as described in Sec. 3.3. Within the synthetic low-light pipeline, we introduce the Video Degradation Profiler Network (VDP-Net) (Sec. 3.2), which generates degradation parameters used to synthesize low-light videos during ELVIS training.

We first train VDP-Net by uniformly sampling degradation parameters ϕ . Once fully trained, VDP-Net can estimate ϕ for any given low-light input. Using these estimated parameters, synthetic low-light videos are then generated through the proposed pipeline, which comprises illumination adjustment, blur, and noise modeling. To train ELVIS, we collect a set of degradation profiles from public real low-light video datasets and synthesize low-light videos on the fly using the proposed low-light degradation model.

3.1. Synthetic Low-Light Video Pipeline

We propose a new unsupervised synthetic low-light pipeline for generating videos to facilitate low-light domain adap-

tation of downstream tasks. This pipeline introduces a novel low-light degradation model that synthesizes low-light videos given a vector of parameters ϕ , estimated by a calibration-free VDP-Net.

Our synthetic low-light video pipeline aims to map videos from normal-light to low-light conditions in a fully unsupervised manner. We denote a video X (with T frames, height H , width W , and C channels) captured under normal lighting as X^{high} , and its corresponding low-light version as X^{low} . The pipeline emulates real video acquisition in digital cameras by modeling exposure, blur, and noise, as illustrated in the yellow panel of Fig. 2.

3.1.1. Illumination adjustment

In the first step of the synthesis procedure, we reduce the illumination of the videos to simulate low-light conditions in the scene. For a linear image representation (e.g., raw sensor data), pixel intensity is directly proportional to scene exposure. Since most images are stored in the sRGB color space, we first convert them to the XYZ color space to ensure linearity. The brightness of a frame \mathbf{x} can then be reduced using the transformation $\mathbf{x}' = \alpha \mathbf{x}$. In photography, a one-stop adjustment in shutter speed, aperture, or ISO corresponds to a doubling or halving of scene exposure; therefore, we rewrite the illumination adjustment function as:

$$X' = 2^\epsilon X, \quad (1)$$

where X' is the darkened video output, ϵ is the exposure adjustment value and X is the input video.

3.1.2. Blur degradation with multivariate Gaussian

We also incorporate blur degradations into our synthetic pipeline—an aspect often overlooked in other synthetic degradation frameworks—despite being a common artifact caused by long shutter speeds, a typical camera setting in

low-light environments. Two types of blur are typically present in low-light videos: motion blur and defocus blur.

Traditionally, linear motion blur is modeled using a line-shaped point spread function (PSF) aligned with the motion direction, while defocus blur is modeled using a Gaussian PSF kernel. An alternative approach to simulating motion blur involves averaging consecutive frames [22, 32, 36, 50]. However, this method offers limited control over blur magnitude, requires small inter-frame motion (thus necessitating high frame rates to avoid ghosting artifacts), discards boundary frames during averaging, and is computationally expensive. Since the effects of motion and defocus blur are difficult to separate, we model their combined effect using a multivariate Gaussian distribution [34]. This approach not only addresses the limitations of frame averaging but also enables VDP-Net to better learn blur degradations with minimal visual discrepancies. As illustrated in Fig. 3, the maximum intensity difference between the traditional method and our approach is less than 4%, indicating very close visual similarity.

We approximate the joint blur kernel H , using three parameters: σ_{H_x} , σ_{H_y} , θ_H , as shown in Eqs. (2) and (3):

$$\Sigma = R \begin{bmatrix} \sigma_{H_x}^2 & 0 \\ 0 & \sigma_{H_y}^2 \end{bmatrix} R^T, R = \begin{bmatrix} \cos \theta_H & -\sin \theta_H \\ \sin \theta_H & \cos \theta_H \end{bmatrix}, \quad (2)$$

$$H[i, j] = \frac{\exp\left(-\frac{1}{2} \mathbf{r}_{ij}^T \Sigma^{-1} \mathbf{r}_{ij}\right)}{\sum_{i,j} \exp\left(-\frac{1}{2} \mathbf{r}_{ij}^T \Sigma^{-1} \mathbf{r}_{ij}\right)}, \quad (3)$$

where i, j refer to the indices of the kernel, Σ is the covariance matrix to determine the spread of the multivariate Gaussian blur kernel, R is the rotation matrix that orientates the 2D Gaussian PSF, and \mathbf{r}_{ij} is the position vector relative to the kernel center. The kernel is normalized such that its sum equals one.

We constrain θ_H to $[0, \frac{\pi}{2}]$ when $\sigma_{H_x} > \sigma_{H_y}$; otherwise, the kernel orientation is assigned to $[\frac{\pi}{2}, \pi]$. Overall, this ensures that the motion-blur kernel angle lies within $[0, \pi]$, because the motion blur kernel is bidirectional (i.e. orientations separated by π radians are equivalent). When σ_{H_x} equals σ_{H_y} , the video exhibits only defocus blur.

3.1.3. Physics-based noise

Our low-light degradation model focuses on physics-based noise arising from the limitations of the camera sensor. We do not consider spatially correlated artifacts introduced or amplified by post-processing steps such as compression, demosaicing, or in-camera denoising, as these are unique to each camera’s image signal processor (ISP).

i) **Read noise** arises from electrical noise present in the signal readout process of the camera sensor. It is a combination of a variety of noise types [40] that can generally be modeled using a Gaussian distribution.

$$N_r \sim \mathcal{N}(0, \sigma_r^2), \quad N_r \in \mathbb{R}^{T \times C \times H \times W}, \quad (4)$$

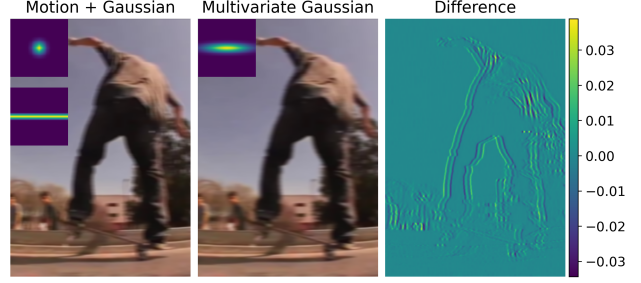


Figure 3. Visual comparison of the linear motion blur + Gaussian blur, the Multivariate Gaussian blur, and the difference between the two resulting images (intensities normalized to $[-1, 1]$). The blur kernels can be seen in the top-left of each blurred image.

where N_r is the read noise map, and σ_r^2 is the variance for the Gaussian distribution.

ii) **Shot noise** is found in low-light capture; resulting from the limited photons hitting the camera sensor from the lack of light in the scene. This behavior can be modeled using a Poisson distribution $\mathcal{P}(\cdot)$

$$(X + N_s) \sim \mathcal{P}\left(\frac{X}{K}\right)K, \quad N_r \in \mathbb{R}^{T \times C \times H \times W}, \quad (5)$$

where N_s is the shot noise map, and K denotes the overall system gain.

iii) **Quantization noise** arises during the process of discretizing the analog signal into a digital signal. This conversion often introduces visual artifacts in the form of grainy or blocky images, which is especially noticeable in images with low bit depth. We model this using a uniform distribution

$$N_q \sim \mathcal{U}(0, \lambda_q), \quad N_q \in \mathbb{R}^{T \times C \times H \times W}, \quad (6)$$

where N_q is the quantization noise map, and λ_q is the upper bound for the quantization noise interval.

iv) **Banding noise**—camera-specific horizontal or vertical lines prominent at high ISO—can be modeled as zero-mean Gaussian noise [31, 40] with standard deviation σ_b controlling band variability. Unlike prior works that model a single orientation, we model *both* for greater flexibility. The banding noise is modeled as

$$N_b \sim \begin{cases} \mathcal{N}(0, \sigma_b^2), & N_b \in \mathbb{R}^{T \times C \times 1 \times W}, \quad \text{if } \theta_b = 0 \\ \mathcal{N}(0, \sigma_b^2), & N_b \in \mathbb{R}^{T \times C \times H \times 1}, \quad \text{if } \theta_b = 1 \end{cases} \quad (7)$$

where N_b is the banding noise map and θ_b determines the orientation of the bands.

3.1.4. Final Low-Light Degradation Model

Combining above degradations, our synthesis function can be expressed as follows:

$$X^{low} = \text{Deg}(X^{high}, \phi) = H * (2^\epsilon X^{high}) + N \quad (8)$$

where $*$ denotes applying a 2D convolution of the kernel H onto video X^{high} , and N is total noise value derived from Eqs. (4) to (7); denoted in a similar fashion to [6, 31, 37, 40]. We define ϕ as a vector of parameters, which are used to apply the degradations onto the video. As such, ϕ can be thought of as a degradation profile.

$$\phi = \{\epsilon, \sigma_r, K, \lambda_q, \sigma_b, \theta_b, \sigma_{H_x}, \sigma_{H_y}, \theta_H\}. \quad (9)$$

3.2. Video Degradation Profiler Network

To estimate the degradation parameters ϕ , we employ our proposed VDP-Net, which efficiently extracts accurate degradation profiles from dark videos without the need for manual calibration. VDP-Net consists of a lightweight feature extractor, a temporal fusion convolutional block, and two multi-layer perceptrons (MLPs) for predicting the degradation parameters.

For the backbone, we use a lightweight pre-trained ResNet-18 [14], which enables faster convergence. Because exposure and noise in low-light video clips are global degradations, whereas blur is a local degradation whose characteristics can vary significantly (particularly in the case of motion blur), we design VDP-Net with two separate prediction heads. The temporal fusion module aggregates features from the backbone along the temporal dimension and passes them to an MLP head to output exposure and noise degradation parameters. The temporal fusion block consists of an average pooling layer, a one-dimensional convolutional layer, batch normalization, and a ReLU activation function.

Unsupervised training strategy. Since real low-light videos lack ground-truth degradation parameters, we adopt an unsupervised training strategy in which random values of ϕ are uniformly sampled to generate degraded inputs X^B for the network. We first consulted domain experts to determine realistic upper bounds for the degradation levels observed in real low-light conditions. During training, values of ϕ within these bounds are passed to our low-light degradation model, together with a clean normal-light video X^A , to synthesize the corresponding low-light video X^B . Uniform sampling ensures that the network learns the full range of degradations without bias.

Loss function. We find that using only the L1 loss between the ground-truth ϕ and the VDP-Net prediction ϕ' is insufficient, particularly for the motion blur parameters. This is because the L1 loss does not account for the cyclical nature of the blur angle. To address this, we introduce a cosine angular loss term that effectively handles this periodic behavior. The overall loss function is defined as

$$\mathcal{L}_{\text{total}} = \lambda_1 |\phi - \phi'|_1 + \lambda_2 (1 - \cos(|\theta_H - \theta'_H|)), \quad (10)$$

where λ_1 and λ_2 are weighting coefficients for each loss component.

3.3. Video Instance Segmentation in ELVIS

3.3.1. Enhancement Decoder Integration

Existing VIS methods [15, 17, 49] are not specifically designed to handle degraded videos and therefore perform poorly, even when retrained on synthetic low-light data, as shown in Fig. 4. To address this limitation, our framework, ELVIS, introduces an enhancement decoder head within the segmentation module of the network. We integrate this decoder into the Mask2Former [8] architecture, which serves as the foundation for many state-of-the-art VIS models.

The proposed enhancement decoder employs a multi-scale deformable attention pixel decoder [51] consisting of ten transformer decoder layers combined with bilinear up-sampling layers to reconstruct normal-light frames. We train the enhanced VIS network by adding an L1 loss between the clean normal-light videos and the decoder’s reconstructed outputs. This additional head maps the latent features of Mask2Former to normal-light representations, guiding the network to disentangle scene content from degradations present in low-light videos.

3.3.2. Training strategy with synthetic low-light data

For VIS training, we first generate a large set of degradation parameters Φ estimated by our VDP-Net across multiple low-light video datasets (SDSD [38], DID [13], BVI-RLV [26], and LMOT [39]). We selected these datasets because they cover a broad range of degradation levels, most of which can be seen in Fig. 5. During VIS training, values of ϕ are randomly sampled from these pre-generated parameters Φ and applied to the input training videos. Collecting Φ in advance, rather than generating them uniformly at random as done when training VDP-Net, enables the VIS model to learn under realistic degradation conditions. This observation is supported by the results in Tab. 3 (4th vs. 5th rows), where our approach achieves more than 16% and 37% improvements in AP and AR, respectively, over the random selection.

4. Experimental Results

We investigated the performance improvements achieved when ELVIS is integrated with several VIS methods across both synthetic and real low-light videos. We also compared our unsupervised synthetic pipeline with existing unsupervised low-light synthesizers by evaluating them on real low-light video instance segmentation and video enhancement tasks.

4.1. VIS Performance

Implementation Details. We selected state-of-the-art (SOTA) VIS methods which incorporate a Mask2Former [8] segmentation head. We trained these using ELVIS on the synthetic YouTube-VIS 2019 [41]

Table 1. Evaluation on the synthetic YouTube-VIS 2019 [41] validation set using several SOTA VIS methods, each trained on synthetic low-light videos generated from the respective training sets with our synthetic pipeline. **Bold** denotes the better performances.

Method	Backbone	AP	AP ₅₀	AP ₇₅	AP _S	AP _M	AP _L	AR ₁	AR ₁₀
MinVIS [17]	ResNet-50	36.4	57.3	36.4	13.3	30.6	49.4	36.5	44.4
GenVIS [15]	ResNet-50	39.1	58.4	42.7	16.2	34.8	55.2	40.3	48.4
DVIS++ [49]	ResNet-50	38.8	59.9	42.8	23.8	38.5	51.4	39.5	49.6
MinVIS [17] + ELVIS	ResNet-50	37.2	57.0	39.6	15.1	34.5	30.9	37.8	45.7
GenVIS [15] + ELVIS	ResNet-50	41.0	59.8	46.2	18.5	38.0	54.2	42.0	51.2
DVIS++ [49] + ELVIS	ResNet-50	42.5	63.8	46.6	27.6	42.5	54.3	41.7	51.9
MinVIS [17]	SWIN-L	51.8	73.8	57.9	28.0	43.0	69.8	46.7	57.5
GenVIS [15]	SWIN-L	53.7	74.8	58.7	27.6	44.9	71.0	49.1	59.6
DVIS++ [49]	ViT-L	55.2	77.2	62.1	29.5	51.6	70.5	49.7	61.5
MinVIS [17] + ELVIS	SWIN-L	54.2	78.3	61.6	28.4	47.6	71.7	49.8	60.1
GenVIS [15] + ELVIS	SWIN-L	55.3	79.3	61.1	26.6	49.6	72.3	49.5	61.2
DVIS++ [49] + ELVIS	ViT-L	56.9	78.7	65.3	25.5	54.3	74.8	50.3	62.7

Table 2. Evaluation on LMOT-S across several SOTA online VIS methods, trained on the synthetic low-light YouTube-VIS 2019 [41] videos from our our synthetic pipeline. **Bold** denotes the better performances.

Method	Backbone	AP	AP ₅₀	AP ₇₅	AR ₁	AR ₁₀
MinVIS [17]	R50	4.1	9.4	2.5	5.2	8.3
GenVIS [15]	R50	5.9	12.2	5.0	5.2	8.3
DVIS++ [49]	R50	6.3	13.3	4.3	4.1	7.9
DVIS++ [49]	ViT-L	8.7	17.1	7.2	5.5	10.4
MinVIS [17] + ELVIS	R50	4.9	11.6	3.2	3.7	5.4
GenVIS [15] + ELVIS	R50	5.9	12.9	4.2	5.1	8.3
DVIS++ [49] + ELVIS	R50	6.9	15.0	4.2	4.6	8.2
DVIS++ [49] + ELVIS	ViT-L	9.1	18.0	8.0	5.5	10.4

Table 3. Evaluation on LMOT-S across different unsupervised synthetic low-light pipelines using GenVIS. **Bold** and underlined denote the best and second-best performers respectively.

Method	AP	AP ₅₀	AP ₇₅	AR ₁	AR ₁₀
Lv <i>et al.</i> [30]	4.2	8.3	4.3	3.5	6.0
Cui <i>et al.</i> [9]	5.4	12.2	4.0	5.1	8.1
Lin <i>et al.</i> [25]	2.5	5.6	1.8	2.8	4.1
Ours (random)	4.2	9.8	2.4	3.1	5.1
Ours	5.9	12.2	5.0	5.2	8.3

dataset by passing its elements into our synthetic low-light pipeline and sampling ϕ from the large degradation profile set Φ . For fair comparison, the benchmark models were also re-trained on synthetic YouTube-VIS 2019.

We evaluate ELVIS on both synthetic and real low-light videos. For the synthetic data experiments, we applied our synthetic pipeline to the YouTube-VIS 2019 validation set (as described above) and evaluated performance using the provided metrics. For the real low-light VIS experiments, since no publicly available datasets currently exist, we evaluated on the sRGB validation set from the Low-light Multi-

Object Tracking (LMOT) dataset [39]. We selected this dataset because it provides both multi-object tracking annotations and aligned normal-light and low-light videos, allowing us to generate segmentation masks within the provided bounding boxes using Segment Anything (SAM) [19] applied to the normal-light videos as pseudo ground truth. We excluded the ‘bicycle’ and ‘bus’ instances to align with the classes used in YouTube-VIS 2019 [41]. The videos were downsampled to 720p and divided into smaller clips for easier processing. We referred to this derived dataset as *LMOT-S* and adopted the same evaluation metrics as YouTube-VIS 2019. Although LMOT-S relied on pseudo ground truth generated by SAM, we considered these results preliminary indicators of the method’s robustness on real-world low-light videos.

Evaluation on synthetic data. We select 3 SOTA VIS methods, MinVIS [17], GenVIS [15] and DVIS++ [49] to demonstrate the versatility of our proposed ELVIS framework; the results are shown in Tab. 1. For MinVIS and GenVIS, we allow the backbones to be finetuned, while for DVIS++, we first train its segmenter network and then we freeze it to train its tracker network. For each of these methods, we use the same training configurations as stated in the respective works. We implement both a CNN backbone and a Transformer backbone to further validate the flexible application of ELVIS. We implement the popular ResNet-50 [14] for the CNN backbone experiments, while for the Transformer backbone experiments, we select the SWIN-L [28] backbone for MinVIS and GenVIS and ViT-L [10] backbone for DVIS++. It is clear that ELVIS improves performances across all metrics; we show significant improvements to AP₅₀ and AP₇₅ demonstrating that our method produces segmentation masks with higher Intersection-over-Union (IoU) accuracy. The improvements to AR show that ELVIS reduces the number of false nega-

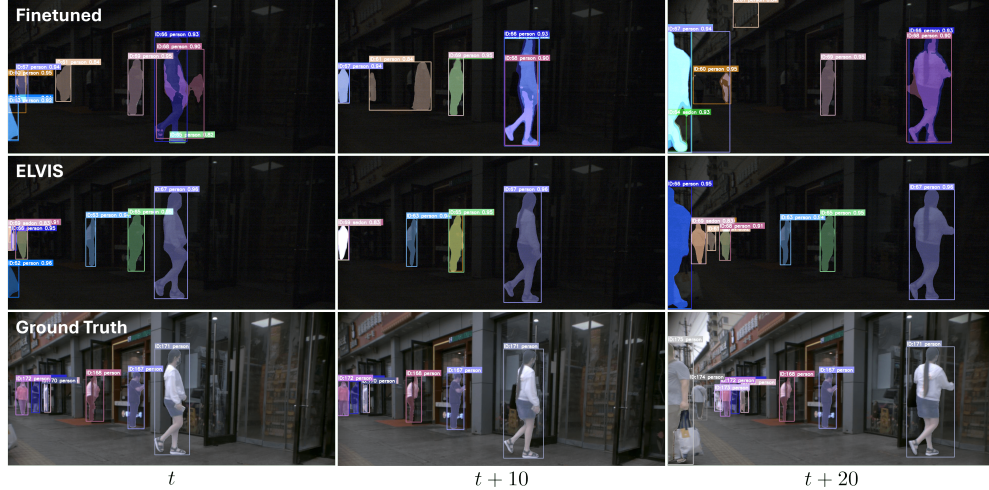


Figure 4. Visual comparison of video instance segmentation results on the LMOT-S dataset using GenVIS [15] method with a ResNet-50 [14] backbone finetuned on our synthetic data (top row) versus implementing our ELVIS framework (middle row), with ground truth (bottom row) for reference. The columns represent frames in the example video, sampled every 10 frames from time t , to show the tracking performances.

tives. Moreover, the increase in AP_M demonstrates that incorporating the enhancement decoder enables the models to better detect and segment medium-sized instances that were previously obscured by low-light degradations.

Evaluation on real low-light data. In our preliminary experiments on real low-light videos, we observe promising improvements in both AP and AR. However, the overall scores in Tab. 2 are noticeably lower than those in Tab. 1, which correspond to the synthetic experiments. This can be attributed to the fact that LMOT-S contains highly challenging scenes with numerous moving instances and severe occlusions, leading to many identity switches (see Supplementary Materials). Nevertheless, we confirm that ELVIS yields qualitative improvements, as shown in Fig. 4, by increasing the number of correct detections while reducing false positives. Moreover, our method decreases the number of identity swaps—a key issue in the LMOT-S benchmark—demonstrating its ability to adapt existing methods to extremely challenging real-world data.

4.2. Comparison of synthetic noise pipelines

We compare our method against other physics-based low-light pipelines [9, 25, 30] used for training VIS models for low-light domain adaptation, with the results shown in Tab. 3. Lin *et al.* [25] propose an unsupervised synthetic low-light pipeline, whereas Lv *et al.* [30] and Cui *et al.* [9] rely on random sampling. We train the baseline GenVIS [15] models with ResNet-50 backbones on synthetic low-light data from YouTube-VIS 2019 dataset [41] using these different pipelines. We also compare against our method by randomly sampling ϕ instead of using the

large set Φ to demonstrate the necessity of VDP-Net. For fairness, all models are evaluated on LMOT-S.

Across all AP metrics, our method used with VDP-Net achieves the best performance and it is only slightly inferior to Cui *et al.*’s [9] method in AR metrics. It should be noted that although our approach does not model spatially correlated noise, unlike [9, 30], it still outperforms others—indicating that in low-light scenes, physics-based degradations have a more dominant impact than spatially correlated noise. Our pipeline with random ϕ shows limited performance; this is likely because the wide range of degradations present requires a longer training period. Examples of the synthesized datasets [13, 38, 39] at different degradation levels are shown in Fig. 5. Each example presents both the synthesized frames (top-right triangle) and their brightened versions (bottom-left triangle) to better visualize the noise. Our pipeline can effectively synthesize a wide range of degradation and noise levels.

4.3. Ablation Study of VDP-Net

Tab. 4 presents an ablation study of various configurations of VDP-Net. For each experiment, we train the model on the synthetic YouTube-VIS 2019 [41] dataset using randomly sampled ϕ values (see Sec. 3.2) for 100 epochs with a batch size of 16. Each input video consists of 5 frames with a patch size of 256×256 pixels. The loss weights are set to $\lambda_1 = 1$ and $\lambda_2 = 1$ when the cosine angular loss (CA loss) is applied. This ablation study analyzes the effects of the temporal fusion block, and the inclusion of CA loss. We evaluate each model on the Real-LOL-Blur [50] dataset, chosen for its wide range of blur levels in low-light frames, allowing us to validate the model’s capability to handle tem-

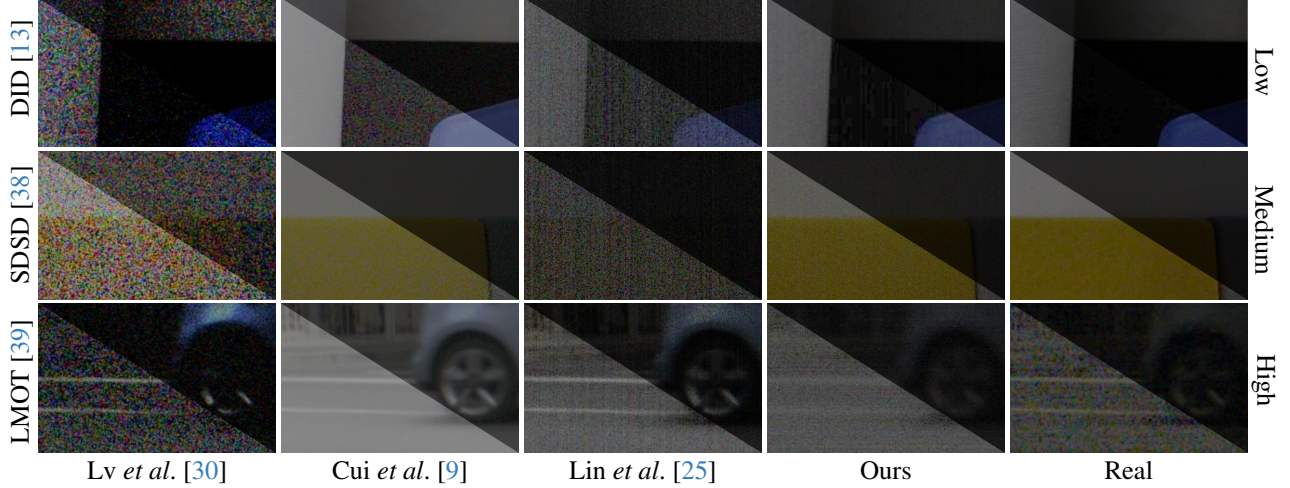


Figure 5. Qualitative analysis of the several synthetic pipelines against the frames from real low-light datasets (SDSD [38], DID [13], LMOT [39]). The brightness and contrast in the bottom-left triangles of each patch were adjusted by 40% for better visibility.

Table 4. Ablation study of VDP-Net components, evaluating CA Loss and Temporal Fusion. The Kullback-Leibler Divergence (KLD) and Fréchet Inception Distance (FID) [16] measure similarity of the synthetic outputs to Real-LOL-Blur [50].

CA Loss	Fusion	KLD ↓	FID ↓
✗	✗	0.573	85.369
✓	✗	0.485	91.100
✓	✓	0.469	85.156

poral degradations. To quantify the distributional differences between synthesized and real low-light frames, we use the Kullback–Leibler Divergence (KLD) [25, 31, 47]. In addition, we measure the perceptual similarity using the Fréchet Inception Distance (FID) [16], a standard metric for measuring the closeness between generated and real image distributions. The results confirm the importance of both the temporal fusion convolution block and the CA loss, as their inclusion leads to consistent reductions in both scores.

4.4. Low-Light Video Enhancement

We further analyze the effectiveness of our synthetic pipeline by comparing it with other synthetic pipelines on low-light video enhancement (LLVE) tasks, using SDSD-Net [38] as the enhancement model. For training, we synthesize the input videos by applying the physics-based synthetic pipelines [9, 25, 30] to the normal-light ground truths from the SDSD [38] and DID [13] datasets for 120k iterations, and evaluate on the corresponding real low-light test sets. We use standard enhancement metrics, including Peak Signal-to-Noise Ratio (PSNR), Structural Similarity Index Measure (SSIM) and the perceptual similarity metric Learned Perceptual Image Patch Similarity (LPIPS) [48]

Table 5. Evaluation of training SDSD-net [38] with physics-based low-light synthetic pipelines across LLVE benchmarks (SDSD [38] and DID [13]) across three metrics PSNR (↑), SSIM (↑) and LPIPS (↓). **Bold** and underlined denote the best and second-best performances respectively.

Method	SDSD			DID		
	PSNR	SSIM	LPIPS	PSNR	SSIM	LPIPS
Lv et al. [30]	15.249	0.399	0.448	12.185	<u>0.580</u>	0.315
Cui et al. [9]	15.684	0.448	0.303	12.220	0.476	<u>0.256</u>
Lin et al. [25]	21.970	0.664	<u>0.285</u>	<u>13.102</u>	0.531	0.351
Ours	<u>16.946</u>	<u>0.611</u>	0.198	14.266	0.676	0.164

for evaluation. As shown in Tab. 5, our method achieves the best performance across all metrics on the DID dataset, and ranks best in LPIPS and second in PSNR/SSIM on SDSD. These results confirm that our synthetic pipeline can effectively generate realistic low-light degradations. Further LLVE analysis is provided in the Supplementary Materials.

5. Conclusion

In this paper we propose ELVIS, the first domain adaptation framework to improve video instance segmentation in the dark. ELVIS provides a new unsupervised synthetic low-light video pipeline which removes the necessity for parameter calibration and adding an additional enhancement decoder module into network architectures to allow the networks to distinguish and disentangle the degradation features from the underlying content. We show that implementing ELVIS into existing SOTA methods boosts VIS performances in low-light videos. While our evaluation on LMOT-S provides preliminary evaluation on real low-light data, we identify the release of properly annotated low-light VIS benchmarks as critical future work for the community.

References

- [1] Martin Arjovsky, Soumith Chintala, and Léon Bottou. Wasserstein generative adversarial networks. In *Proceedings of the 34th International Conference on Machine Learning*, pages 214–223. PMLR, 2017. 2
- [2] Jong-Hyeon Baek, Jiwon Oh, and Yeong Jun Koh. Evolve: Event-guided deformable feature transfer and dual-memory refinement for low-light video object segmentation. In *Proceedings of the IEEE/CVF International Conference on Computer Vision (ICCV)*, pages 11273–11282, 2025. 2
- [3] Jiesong Bai, Yuhao Yin, Qiyuan He, Yuanxian Li, and Xiaofeng Zhang. Retinexmamba: Retinex-based mamba for low-light image enhancement. In *Neural Information Processing*, pages 427–442, Singapore, 2025. Springer Nature Singapore. 1
- [4] Tim Brooks, Ben Mildenhall, Tianfan Xue, Jiawen Chen, Dillon Sharlet, and Jonathan T Barron. Unprocessing images for learned raw denoising. In *IEEE Conference on Computer Vision and Pattern Recognition (CVPR)*, 2019. 2, 3
- [5] Yuanhao Cai, Hao Bian, Jing Lin, Haoqian Wang, Radu Timofte, and Yulun Zhang. Retinexformer: One-stage retinex-based transformer for low-light image enhancement. In *Proceedings of the IEEE/CVF International Conference on Computer Vision (ICCV)*, pages 12504–12513, 2023. 1
- [6] Yue Cao, Ming Liu, Shuai Liu, Xiaotao Wang, Lei Lei, and Wangmeng Zuo. Physics-guided iso-dependent sensor noise modeling for extreme low-light photography. In *Proceedings of the IEEE/CVF Conference on Computer Vision and Pattern Recognition (CVPR)*, pages 5744–5753, 2023. 5
- [7] Linwei Chen, Ying Fu, Kaixuan Wei, Dezhi Zheng, and Felix Heide. Instance segmentation in the dark. *International Journal of Computer Vision*, 131(8):2198–2218, 2023. 2, 3
- [8] Bowen Cheng, Ishan Misra, Alexander G. Schwing, Alexander Kirillov, and Rohit Girdhar. Masked-attention mask transformer for universal image segmentation. In *Proceedings of the IEEE/CVF Conference on Computer Vision and Pattern Recognition (CVPR)*, pages 1290–1299, 2022. 5
- [9] Ziteng Cui, Guo-Jun Qi, Lin Gu, Shaodi You, Zenghui Zhang, and Tatsuya Harada. Multitask aet with orthogonal tangent regularity for dark object detection. In *Proceedings of the IEEE/CVF International Conference on Computer Vision (ICCV)*, pages 2553–2562, 2021. 1, 2, 6, 7, 8
- [10] Alexey Dosovitskiy, Lucas Beyer, Alexander Kolesnikov, Dirk Weissenborn, Xiaohua Zhai, Thomas Unterthiner, Mostafa Dehghani, Matthias Minderer, Georg Heigold, Sylvain Gelly, Jakob Uszkoreit, and Neil Houlsby. An image is worth 16x16 words: Transformers for image recognition at scale. In *International Conference on Learning Representations*, 2021. 6
- [11] Zhipeng Du, Miaoqing Shi, and Jiankang Deng. Boosting object detection with zero-shot day-night domain adaptation. In *Proceedings of the IEEE/CVF Conference on Computer Vision and Pattern Recognition (CVPR)*, pages 12666–12676, 2024. 2
- [12] Alessandro Foi, Mejdi Trimeche, Vladimir Katkovnik, and Karen Egiazarian. Practical poissonian-gaussian noise modeling and fitting for single-image raw-data. *IEEE Transactions on Image Processing*, 17(10):1737–1754, 2008. 2
- [13] Huiyuan Fu, Wenkai Zheng, Xicong Wang, Jiaxuan Wang, Heng Zhang, and Huadong Ma. Dancing in the dark: A benchmark towards general low-light video enhancement. In *Proceedings of the IEEE/CVF International Conference on Computer Vision (ICCV)*, pages 12877–12886, 2023. 5, 7, 8, 1, 2
- [14] Kaiming He, Xiangyu Zhang, Shaoqing Ren, and Jian Sun. Deep residual learning for image recognition. In *2016 IEEE Conference on Computer Vision and Pattern Recognition (CVPR)*, pages 770–778, 2016. 5, 6, 7
- [15] Miran Heo, Sukjun Hwang, Jeongseok Hyun, Hanjung Kim, Seoung Wug Oh, Joon-Young Lee, and Seon Joo Kim. A generalized framework for video instance segmentation. In *CVPR*, 2023. 1, 5, 6, 7, 2
- [16] Martin Heusel, Hubert Ramsauer, Thomas Unterthiner, Bernhard Nessler, and Sepp Hochreiter. Gans trained by a two time-scale update rule converge to a local nash equilibrium. In *Advances in Neural Information Processing Systems*. Curran Associates, Inc., 2017. 8
- [17] De-An Huang, Zhiding Yu, and Anima Anandkumar. Minvis: A minimal video instance segmentation framework without video-based training. In *Advances in Neural Information Processing Systems*, pages 31265–31277. Curran Associates, Inc., 2022. 5, 6
- [18] Xin Jin, Jia-Wen Xiao, Ling-Hao Han, Chunle Guo, Ruixun Zhang, Xialei Liu, and Chongyi Li. Lighting every darkness in two pairs: A calibration-free pipeline for raw denoising. In *Proceedings of the IEEE/CVF International Conference on Computer Vision (ICCV)*, pages 13275–13284, 2023. 2
- [19] Alexander Kirillov, Eric Mintun, Nikhila Ravi, Hanzi Mao, Chloe Rolland, Laura Gustafson, Tete Xiao, Spencer Whitehead, Alexander C. Berg, Wan-Yen Lo, Piotr Dollár, and Ross Girshick. Segment anything. *arXiv:2304.02643*, 2023. 6
- [20] Edwin H Land. The retinex theory of color vision. *Scientific american*, 237(6):108–129, 1977. 3
- [21] Sohyun Lee, Jaesung Rim, Boseung Jeong, Geonu Kim, Byungju Woo, Haechan Lee, Sunghyun Cho, and Suha Kwak. Human pose estimation in extremely low-light conditions. In *Proceedings of the IEEE/CVF Conference on Computer Vision and Pattern Recognition (CVPR)*, pages 704–714, 2023. 1
- [22] Dongxu Li, Chenchen Xu, Kaihao Zhang, Xin Yu, Yiran Zhong, Wenqi Ren, Hanna Suominen, and Hongdong Li. Arvo: Learning all-range volumetric correspondence for video deblurring. In *Proceedings of the IEEE/CVF Conference on Computer Vision and Pattern Recognition (CVPR)*, pages 7721–7731, 2021. 4
- [23] Hebei Li, Jin Wang, Jiahui Yuan, Yue Li, Wenming Weng, Yansong Peng, Yueyi Zhang, Zhiwei Xiong, and Xiaoyan Sun. Event-assisted low-light video object segmentation. In *Proceedings of the IEEE/CVF Conference on Computer Vision and Pattern Recognition (CVPR)*, pages 3250–3259, 2024. 1, 2
- [24] Joanne Lin, Nantheera Anantrasirichai, and David Bull. Multi-scale denoising in the feature space for low-light in-

- stance segmentation. In *ICASSP 2025 - 2025 IEEE International Conference on Acoustics, Speech and Signal Processing (ICASSP)*, pages 1–5, 2025. 1, 2
- [25] Joanne Lin, Crispian Morris, Ruirui Lin, Fan Zhang, David Bull, and Nantheera Anantrasirichai. Towards a general-purpose zero-shot synthetic low-light image and video pipeline. In *Proceedings of the 3rd International Workshop on Multimedia Content Generation and Evaluation: New Methods and Practice*, page 3–11, New York, NY, USA, 2025. Association for Computing Machinery. 2, 6, 7, 8, 1
- [26] R Lin, N Anantrasirichai, G Huang, J Lin, Q Sun, A Malyugina, and DR Bull. BVI-RLV: A fully registered dataset and benchmarks for low-light video enhancement. *arXiv preprint arXiv:2407.03535*, 2024. 1, 5
- [27] Yu Liu, Arif Mahmood, and Muhammad Haris Khan. Nt-vot211: A large-scale benchmark for night-time visual object tracking. In *Proceedings of the Asian Conference on Computer Vision (ACCV)*, pages 194–212, 2024. 1
- [28] Ze Liu, Yutong Lin, Yue Cao, Han Hu, Yixuan Wei, Zheng Zhang, Stephen Lin, and Baining Guo. Swin transformer: Hierarchical vision transformer using shifted windows. In *Proceedings of the IEEE/CVF International Conference on Computer Vision (ICCV)*, pages 10012–10022, 2021. 6
- [29] Rundong Luo, Wenjing Wang, Wenhan Yang, and Jiaying Liu. Similarity min-max: Zero-shot day-night domain adaptation. In *Proceedings of the IEEE/CVF International Conference on Computer Vision (ICCV)*, pages 8104–8114, 2023. 2
- [30] Feifan Lv, Yu Li, and Feng Lu. Attention guided low-light image enhancement with a large scale low-light simulation dataset. *International Journal of Computer Vision*, 129(7): 2175–2193, 2021. 2, 6, 7, 8, 1
- [31] Kristina Monakhova, Stephan R. Richter, Laura Waller, and Vladlen Koltun. Dancing under the stars: Video denoising in starlight. In *Proceedings of the IEEE/CVF Conference on Computer Vision and Pattern Recognition (CVPR)*, pages 16241–16251, 2022. 2, 4, 5, 8
- [32] Seungjun Nah, Tae Hyun Kim, and Kyoung Mu Lee. Deep multi-scale convolutional neural network for dynamic scene deblurring. In *Proceedings of the IEEE Conference on Computer Vision and Pattern Recognition (CVPR)*, 2017. 4
- [33] Simon Niklaus, Long Mai, and Feng Liu. Video frame interpolation via adaptive separable convolution. In *IEEE International Conference on Computer Vision*, 2017. 2
- [34] Alberto Pretto, Emanuele Menegatti, Maren Bennewitz, Wolfram Burgard, and Enrico Pagello. A visual odometry framework robust to motion blur. In *2009 IEEE International Conference on Robotics and Automation*, pages 2250–2257, 2009. 4
- [35] Olaf Ronneberger, Philipp Fischer, and Thomas Brox. U-net: Convolutional networks for biomedical image segmentation. In *Medical Image Computing and Computer-Assisted Intervention – MICCAI 2015*, pages 234–241, Cham, 2015. Springer International Publishing. 2
- [36] Shuochen Su, Mauricio Delbracio, Jue Wang, Guillermo Sapiro, Wolfgang Heidrich, and Oliver Wang. Deep video deblurring for hand-held cameras. In *Proceedings of the IEEE Conference on Computer Vision and Pattern Recognition (CVPR)*, 2017. 4
- [37] Jing Wang, Yitong Yu, Songtao Wu, Chang Lei, and Kuanhong Xu. Rethinking noise modeling in extreme low-light environments. In *2021 IEEE International Conference on Multimedia and Expo (ICME)*, pages 1–6, 2021. 2, 5
- [38] Ruixing Wang, Xiaogang Xu, Chi-Wing Fu, Jiangbo Lu, Bei Yu, and Jiaya Jia. Seeing dynamic scene in the dark: High-quality video dataset with mechatronic alignment. In *ICCV*, 2021. 1, 5, 7, 8, 2
- [39] Xinzhe Wang, Kang Ma, Qiankun Liu, Yunhao Zou, and Ying Fu. Multi-object tracking in the dark. In *Proceedings of the IEEE/CVF Conference on Computer Vision and Pattern Recognition (CVPR)*, pages 382–392, 2024. 1, 5, 6, 7, 8
- [40] Kaixuan Wei, Ying Fu, Yinqiang Zheng, and Jiaolong Yang. Physics-based noise modeling for extreme low-light photography. *IEEE Transactions on Pattern Analysis and Machine Intelligence*, 44(11):8520–8537, 2021. 2, 3, 4, 5
- [41] Linjie Yang, Yuchen Fan, and Ning Xu. Video instance segmentation. In *ICCV*, 2019. 5, 6, 7, 1
- [42] Zhen Yao and Mooi Choo Chuah. Event-guided low-light video semantic segmentation. In *Proceedings of the Winter Conference on Applications of Computer Vision (WACV)*, pages 3330–3341, 2025. 2
- [43] Junjie Ye, Changhong Fu, Ziang Cao, Shan An, Guangze Zheng, and Bowen Li. Tracker Meets Night: A Transformer Enhancer for UAV Tracking. *IEEE Robotics and Automation Letters*, 7(2):3866–3873, 2022. 1
- [44] Anqi Yi and Nantheera Anantrasirichai. A comprehensive study of object tracking in low-light environments. *arXiv:2312.16250*, 2024. 1
- [45] Syed Waqas Zamir, Aditya Arora, Salman Khan, Munawar Hayat, Fahad Shahbaz Khan, Ming-Hsuan Yang, and Ling Shao. Cycleisp: Real image restoration via improved data synthesis. In *Proceedings of the IEEE/CVF Conference on Computer Vision and Pattern Recognition (CVPR)*, 2020. 2
- [46] Fan Zhang, Yu Li, Shaodi You, and Ying Fu. Learning temporal consistency for low light video enhancement from single images. In *Proceedings of the IEEE/CVF Conference on Computer Vision and Pattern Recognition (CVPR)*, pages 4967–4976, 2021. 2
- [47] Feng Zhang, Bin Xu, Zhiqiang Li, Xinran Liu, Qingbo Lu, Changxin Gao, and Nong Sang. Towards general low-light raw noise synthesis and modeling. In *Proceedings of the IEEE/CVF International Conference on Computer Vision (ICCV)*, pages 10820–10830, 2023. 8
- [48] Richard Zhang, Phillip Isola, Alexei A Efros, Eli Shechtman, and Oliver Wang. The unreasonable effectiveness of deep features as a perceptual metric. In *CVPR*, 2018. 8
- [49] Tao Zhang, Xingye Tian, Yikang Zhou, Shunping Ji, Xuebo Wang, Xin Tao, Yuan Zhang, Pengfei Wan, Zhongyuan Wang, and Yu Wu. Dvis++: Improved decoupled framework for universal video segmentation. *IEEE Transactions on Pattern Analysis and Machine Intelligence*, 47(7):5918–5929, 2025. 5, 6
- [50] Shangchen Zhou, Chongyi Li, and Chen Change Loy. Led-net: Joint low-light enhancement and deblurring in the dark. In *ECCV*, 2022. 2, 4, 7, 8

- [51] Xizhou Zhu, Weijie Su, Lewei Lu, Bin Li, Xiaogang Wang, and Jifeng Dai. Deformable {detr}: Deformable transformers for end-to-end object detection. In *International Conference on Learning Representations*, 2021. [5](#)
- [52] Yunhao Zou, Ying Fu, Yulun Zhang, Tao Zhang, Chenggang Yan, and Radu Timofte. Calibration-free raw image denoising via fine-grained noise estimation. *IEEE Transactions on Pattern Analysis and Machine Intelligence*, 47(7): 5368–5384, 2025. [2](#)

ELVIS: Enhance Low-light for Video Instance Segmentation in the Dark

Supplementary Material

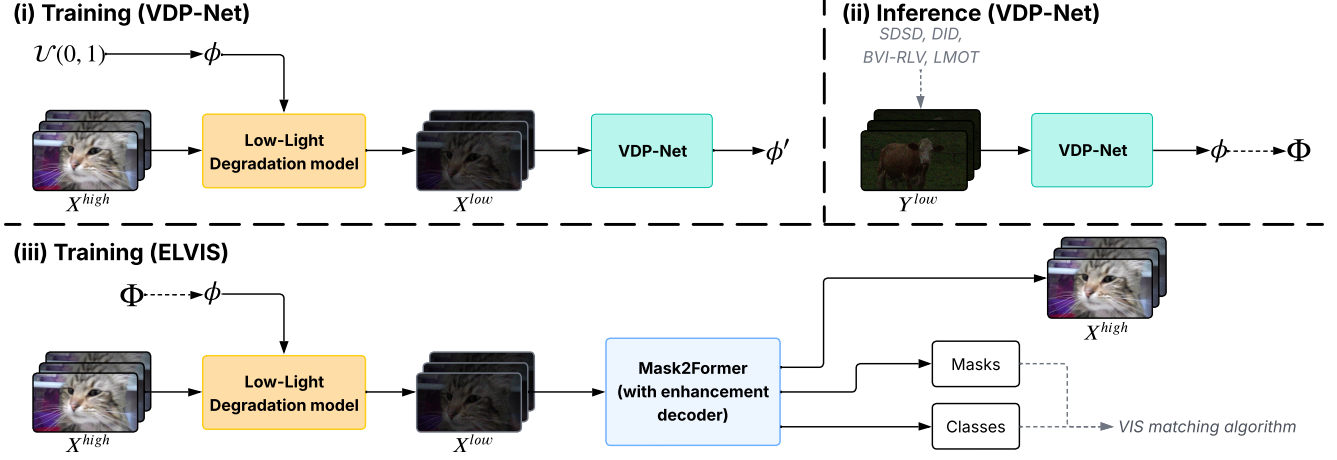


Figure S1. Step-by-step process for using the ELVIS framework: (i) train VDP-Net to predict degradation profile ϕ , (ii) build Φ from real low-light datasets [13, 26, 38, 39], and (iii) use degradation profiles from Φ to create synthetic data to train ELVIS.

S1. ELVIS details

Fig. S1 shows a step-by-step visualization of each process required for the ELVIS framework for clarity. Refer to the main paper for the implementation details of each step.

S2. Real Low-Light VIS performances

Although LMOT-S [39] offers a useful preliminary evaluation for real-world settings, it is a far more challenging benchmark than YouTube-VIS 2019 [41]. One main reason for the notably lower performances in Tab. 2 can be attributed to the instance counts (see Tab. S1). LMOT-S contains at least 9 instances per video, whereas the YouTube-VIS 2019 validation set contains at most 6; existing VIS methods trained on YouTube-VIS 2019 are not designed to handle such large number of instances.

Another challenge is the cross-over issue, which leads to a high number of identity switches. Combined with the fact that these methods are designed to track far fewer instances, this results in frequent identity switches and a failure to form new tracklets. An example can be seen in Fig. S2, where in the finetuned GenVIS [15] model, it transferred the sedan identity (ID: 196) onto the motorcycle as it drove past the car, and created a new identity (ID: 193) for the car. ELVIS reduces the occurrences of such issues, but they still persist (see the truck in frame t). In Tab. S2, we also compare against GenVIS with off-the-shelf weights provided by the authors, on the paired normal-light frames of LMOT-S, to emphasize the limitations of the benchmark.

Table S1. Statistics of count of instances from YouTube-VIS [41] versus LMOT-S validation sets

Dataset	Min	Max	Mean
YouTube-VIS 2019 [41]	1	6	1.7
LMOT-S	9	75	31.5

Table S2. LMOT-S results on GenVIS [15] (ResNet-50) trained on our synthetic low-light YouTube-VIS 2019 videos, with detection increased to 100. Original pretrained normal-light results are shown for comparison.

Method	Light	AP	AP ₅₀	AP ₇₅	AR ₁	AR ₁₀	AR ₁₀₀
GenVIS [15]	Low	6.6	14.5	5.2	5.4	9.8	11.7
GenVIS [15] + ELVIS	Low	6.7	15.5	4.4	5.3	12.1	14.0
GenVIS [15] (pre-trained)	Normal	11.7	21.4	10.5	8.8	16.8	21.0

Table S3. Evaluation of SDSD-net [38] trained with physics-based low-light synthetic pipelines on LLVE benchmarks (SDSD [38], DID [13]) using PSNR (\uparrow), SSIM (\uparrow), and LPIPS (\downarrow). Outputs are histogram-matched. **Bold** indicates the best results.

Method	PSNR	SDSD SSIM	LPIPS	PSNR	DID SSIM	LPIPS
Lv <i>et al.</i> [30]	21.421	0.464	0.563	16.606	0.846	0.476
Cui <i>et al.</i> [9]	19.199	0.645	0.380	22.042	0.824	0.220
Lin <i>et al.</i> [25]	23.088	0.645	0.393	17.354	0.624	0.450
Ours	20.703	0.688	0.282	22.794	0.846	0.197

S3. Low-Light Video Enhancement Results

We find that the outputs from SDSD-net [38] show severe artifacts (see Fig. S3 and Fig. S4); this is an observation

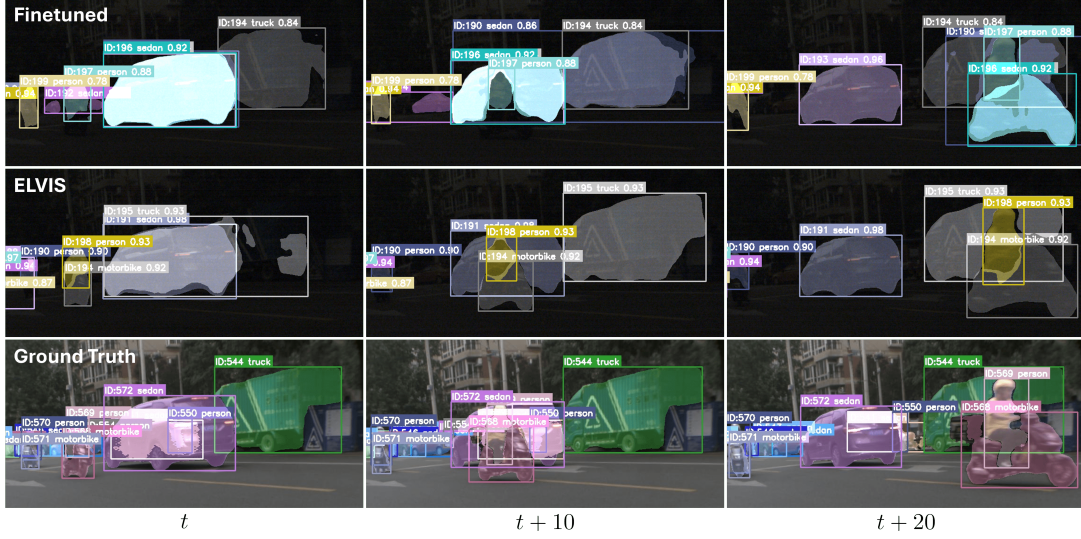


Figure S2. Visual comparison of segmentation and tracking success and failure cases on the LMOT-S dataset using GenVIS [15] method with a ResNet-50 backbone finetuned on our synthetic data (top row) versus implementing our ELVIS framework (middle row), with ground truth (bottom row) for reference. The columns represent frames in the example video, sampled every 10 frames from time t , to show the tracking performances.

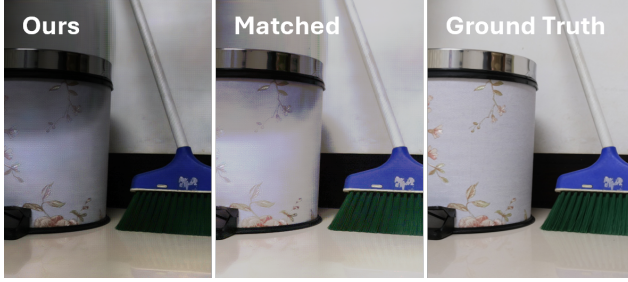


Figure S3. Example of artifacts in the enhanced output which is not removed with histogram matching. (Left) the enhanced output from SDSNet [38] trained on our synthetic pipeline. (Center) the histogram-matched output to the ground truth. (Right) is the ground truth normal-exposed frame.

also mentioned by Fu *et al.* [13]. This explains the modest performances across all synthetic pipelines in Tab. 5. For further analysis, we conduct additional LLVE experiments focusing on the denoising component of SDSNet by using different synthetic training data. Before computing the evaluation metrics, we apply histogram matching between the enhanced outputs and the ground truths. The results reflect the noise synthesis accuracy of each method. The results are shown in Tab. S3. While PSNR and SSIM show noticeable improvements, we find that LPIPS scores worsen with histogram matching, likely because it can amplify the artifacts, reducing perceptual similarity. We would like to mention that histogram matching is not the perfect solution for alleviating the artifacts in evaluation (see Fig. S3).

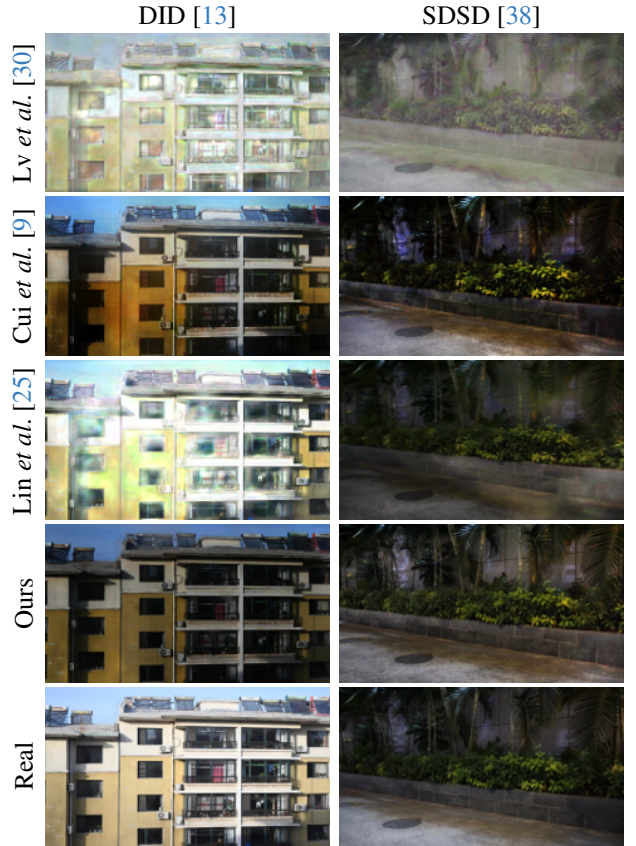


Figure S4. Qualitative comparison of the enhanced outputs of SDSnet [38] trained on different synthetic pipelines from the SDSNet [38] and DID [13] datasets.